Solder Joint Failures under Thermo-Mechanical Loading Conditions – A Review

Joshua Depiver[1, a], Sabuj Mallik[1, b] and Dani Harmanto[1, c]

[1]Department of Mechanical Engineering & Built Environment, College of Engineering & Technology

University of Derby, Markeaton Street, Derby, DE22 3AW, United Kingdom

[a]j.depiver@derby.ac.uk , [b]s.mallik@derby.ac.uk, [c]d.harmanto@derby.ac.uk

Abstract. Solder joints play a critical role in electronic devices by providing electrical, mechanical and thermal interconnections. These miniature joints are also the weakest links in an electronic device. Under severe thermal and mechanical loadings, solder joints could fail in 'tensile fracture' due to stress overloading, 'fatigue failure' because of the application of cyclical stress and 'creep failure' due to a permanent long-term load. This paper reviews the literature on solder joint failures under thermo-mechanical loading conditions, with a particular emphasis on fatigue and creep failures. Literature reviews mainly focused on commonly used lead-free Sn-Ag-Cu (SAC) solders. Based on literature in experimental and simulation studies on solder joints, it was found that fatigue failures are widely induced by accelerated thermal cycling (ATC). During ATC, the mismatch in coefficients of thermal expansion (CTE) between different elements of electronics assembly contributes significantly to induce thermal stresses on solder joints. The fatigue life of solder joints is predicted based on phenomenological fatigue models that utilise materials properties as inputs. A comparative study of 14 different fatigue life prediction models is presented with their relative advantages, scope and limitations. Creep failures in solder joints, on the other hand, are commonly induced through isothermal ageing. A critical review of various creep models is presented. Many of these strain rate-based creep models are routed to very well-known Anand Model of inelastic strain rate. Finally, the paper outlined the combined effect of creep and fatigue on solder joint failure.

Keywords: solder joint, creep failure, fatigue failure, thermal cycling, thermal ageing

1.0 Introduction

In electronics packaging, solder joints provide the essential mechanical and electrical connections between package elements and substrate. These joints also serve as the weakest links in the overall package in the sense that if any of these joints fail then the whole system could eventually fail and stop functioning. From a structural point of view, solder joints are heterogeneous and dynamic systems, and it is essential to study various elements of the solder structure, to understand their thermo-mechanical behaviours. During operation, electronic products are exposed to a variety of application conditions such as vibration, which can cause impact and fatigue failures. Thermal ageing of solder joints, on the other hand, induces changes in solder microstructure and could trigger creep failure [1, 2]. Knowledge and understanding of failure of these systems are critical to averting accidents, which may result, in life or death and profit or loss associated costs [3].

The reliability of electronic devices has become very significant for the operational performance of electronics systems used in safety-critical applications such as automobile, aeroplane, oil & gas drilling applications, defence, power grids, medical devices and so forth. Because solder joints are small and employed at high temperatures, the reliability of solder joint is of ultimate concern to electronics manufacturing engineers. Solder joint reliability is defined as the capability of solder joints to remain in conformance with their electrical, visual and mechanical specifications over a specified period, under a detailed set of operational conditions. Reliability of these joints is influenced by various factors such as creep resistance, thermal fatigue resistance, shear strength, drop shock, and vibration resistance. Due to the adoption of the Restriction of Hazardous Substances (RoHS) directives in July 2006, there have been new advancements and developments in lead-free solders as

a substitute for the conventional lead-based solders, for use in the electronics manufacturing industries [4-8]. Amongst the lead-free solders investigated, Sn-Ag and Sn-Ag-Cu based solders offer the most promising characteristics as replacement of lead-based solders [9, 10]. Introduction of new lead-free solders added a new dimension to reliability issues in electronic devices.

The existence of intermetallic compounds (IMCs) in solder joints results in improved mechanical properties and can be enhanced by grain refinement and precipitate strengthening mechanisms [11, 12]. However, the brittle nature of bulk IMC [13] and low creep resistance [14] are two significant drawbacks of these solders, while in service for high-density devices. Thermo-mechanical fatigue occurs because most electronic packages consisted of a variety of materials with different coefficients of thermal expansion (CTE) and exposed to thermal fluctuations as a result of internal heating or ambient temperature changes. As a result of thermal and mechanical stresses, solder microstructure develops a weaker coarsened structure, and formation of brittle IMCs (through interfacial reactions) are accelerated. Both thermo-mechanical fatigue and thermal ageing pose a significant threat to the long-term reliability of solder interconnects. In order to understand how reliable these interconnects are, metallurgical changes that affect characteristics of solder interconnect, such as bond formation, creep and fatigue behaviour must be fully understood [15-20].

Solder joint failures take place for many reasons, such as a) weak solder joint design; b) weak solder joint processing; c) solder material issues; d) excessive stresses applied to the solder joints and many more. In general, however, solder joint failures are merely ranked according to the characteristics of the stresses that applied to them, as well as the way the solder joints fail. The prominent failure concerns for solder joints are thermal cycling durability, creep deformation, mechanical cycling, vibration durability, solder joint ageing, stress overloading, fatigue, intermetallic growth, and electro and electrochemical migration. Understanding the physics of these failure mechanisms supports reliability improvement and evaluation [21]. Several solder joint failures occur under three significant categories: 1) fatigue failure as a result of the application of cyclical stresses; 2) creep failure due to the application of a long-term, permanent load; and 3) tensile fracture due to stress overloading, which is short-term. It should be known moreover that more than one of these stresses can act on a solder joint in any given circumstance. Degradation of solder joint by factors such as corrosion needs to be considered as well.

A detailed understanding of the thermo-mechanical behaviour of lead-free solder interconnect is vital in improving operational reliability. Numerous experimental studies were carried out to evaluate solder joint reliability, as evident from studies carried out by Chen & Chen [22] and Forde et al. [23]. A number of research studies [24-29] have also focused on the formation of IMC and its effect on the initiation and propagation behaviours of fatigue cracks and creep failures; and how those lead to the phenomenon of stress concentration, where cracks began to sprout and gradually extend. Relevant literature shows that the service life, reliability and performance of electronic products are greatly influenced by temperature which results in failures [30-32]. The emphasis of this paper is to examine the solder joint fatigue and creep failures under thermo-mechanical loading conditions.

2.0 Solder Joints Fatigue Failure

2.1 Thermal Fatigue Failure models for Solder Joints

Thermal fatigue is a leading cause of failure of solder joints in surface mount electronic components, and it is significant in high-reliability applications such as in telecommunication, military, and aeronautics. In electronic assemblies, however, solder joints usually experience thermal stresses because of combined effects of non-uniform temperature distributions in the package and a mismatch in CTE between the component and substrate material. Thermo-mechanical fatigue arises when

materials with different characteristic CTEs are joined and used in an environment that experiences cyclic temperature fluctuations resulting in imposed cycling strain. Fig. 1 shows a solder joint with fatigue failure, mounted on a printed circuit board (PCB) [33]. Choi & Dasgupta [34] investigated the fatigue of solder interconnects in microelectronic assemblies under random vibration. They applied the well-known Coffin-Manson fatigue model and rainflow cycle counting to measure model constants and to compare fatigue damage accumulation rates under harmonic versus electro-dynamic (ED) random vibration excitation. They focused on solder durability and strain response under random and harmonic vibration loading, based on experiments and modelling. Multiscale finite element modelling (FEM) is required to address the vibration response of complex electronic assemblies. An analysis was conducted by the researchers in the time domain to manage the nonlinear material behaviour of solder. Their conclusions focus on solder strain response and durability under random and harmonic vibration loading, based on experiments and modelling. Multiscale FEM is required to address the vibration response of complex electronic assemblies.

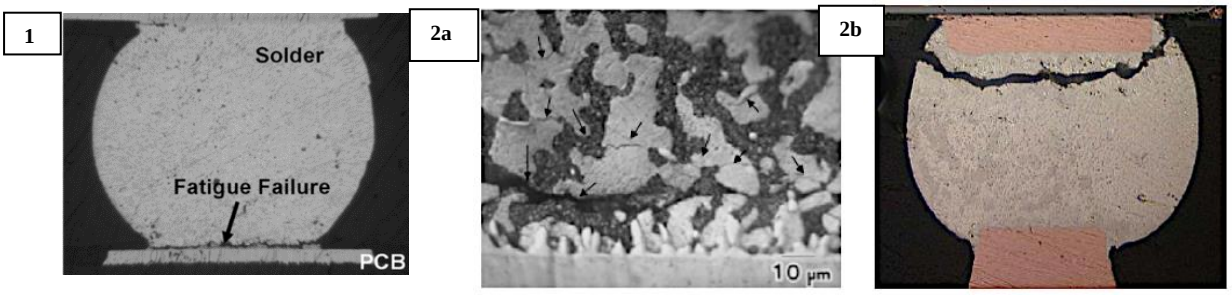

Figure 1: Solder joint fatigue failure [33]; Figure 2: (a) Cracks propagate through the Sn-rich phase at Sn-Sn grain boundaries after thermo-mechanical fatigue (b) Optical micrograph of a failed Sn-3.5Ag solder joint after experiencing thermo-mechanical fatigue [35]

Even small fluctuations of operating temperature can have a significant impact on solder integrity, due to CTE mismatch between connected components. Following a critical number of thermal excursions, such as the machine on/off cycles, solder joints encounter fatigue failure. The type and significance of strains in solder joints under conditions of thermo-mechanical fatigue are often quite complex. For surface mount applications, the strain is nominally in shear. Nonetheless, tensile and mixed-mode strains can occur due to bending of the chip carrier or board. Fig. 2(a) is showing the microstructure of a failed solder joint, adapted from ref [35]. The heterogeneously coarsened colony boundaries are weaker than the rest of the joint and any additional deformation concentrates in the coarsened regions resulting in further coarsening. Failure finally happens because of cracks that form in the coarsened regions of the joint. Other solder alloys, such as the lead-free Sn-3.5Ag eutectic-based solders, experience thermal and mechanical fatigue damage and failure at tin grain boundaries, as presented in Fig. 2(b) [35].

Thermal stresses can also be induced because of a mismatch in the CTE between different constituents of the assembly. However, in electronic assemblies, solder joints usually experience thermal stresses due to non-uniform temperature distributions in the package and a mismatch in CTE between the component and substrate material [35-37]. Coyle et al. [38] investigated the thermal fatigue characteristics of Pb-free solder joints. A significant finding from their study is that positive impact of Ag on accelerated thermal cycling (ATC) reliability (measured by characteristic lifetime) reduces as the harshness of the ATC (expressed by higher ΔT, advanced peak temperature, and lengthier dwell time) increases. The outcomes also show that all the Pb-free solders are more dependable in accelerated thermal cycling than the SnPb alloy they have substituted [39, 40]. Li et al. [28] reviewed typical thermal fatigue failure models for solder joints of electronic components. They examined several classifications of thermal fatigue failure models of the solder joint in electronics components as shown in the Fig. 3.

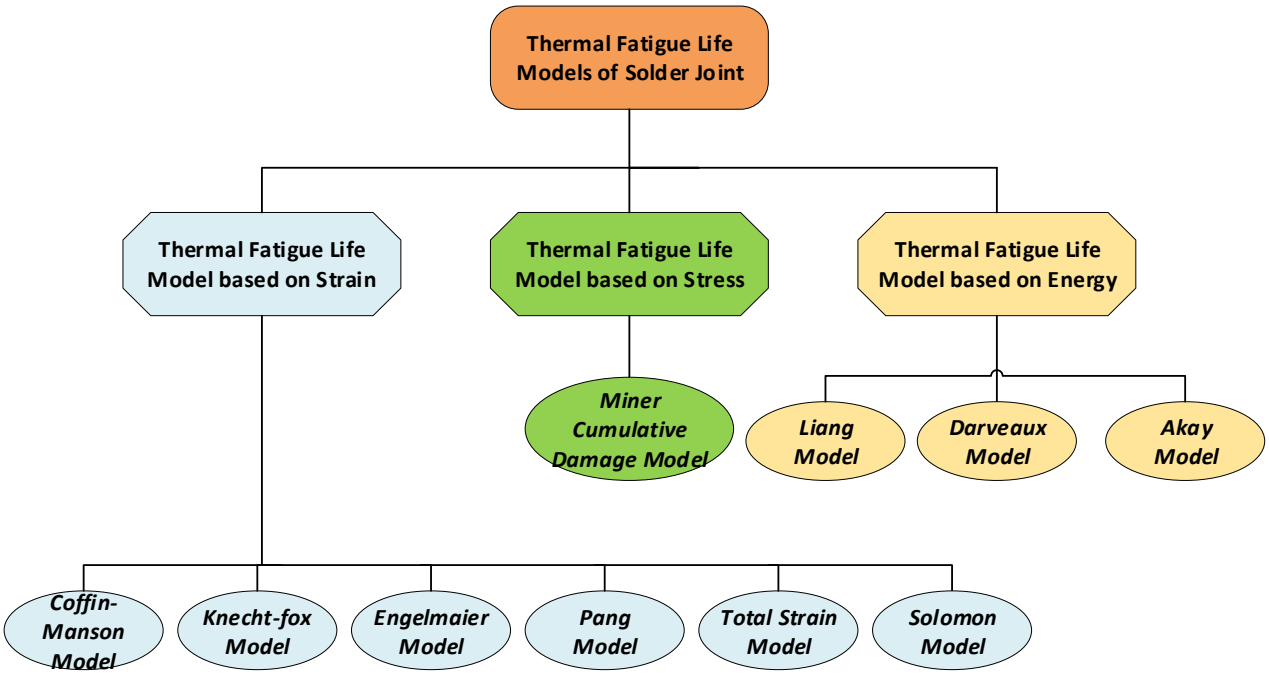

Figure 3: Thermal fatigue life model of solder joints [Adapted ref: 28]

Petrone et al [41] carried out a steady thermo-mechanical analysis for a surface-mount electronic device, as shown in Fig. 4 (a). Fig. 4(b) presents the effective plastic strain distribution for SAC305. A copper frame essentially makes the device, a lead-free solder layer (solder die) and silicon die equipped with a front metal, which is connected to devise pins by several ribbons. Continuous equations were spatially discretised by a finite element approach based on the Galerkin technique on non-uniform and non-structured computational grids made of tetrahedral Lagrange elements of order 2. Influence of spatial discretisation was preliminarily studied to guarantee mesh-independent effects. Subsequently, a computational network composed of about 45,250 elements was preserved for calculations, generating 137,399 degrees of freedom. The thermal distribution results obtained from the study are presented in Fig. 5 (a) and (b). The thermo-mechanical analysis shows the von Mises stress distribution, triggered by the thermal cycling, shown in Fig. 5 (b). A snap view of the applied mesh is presented in Fig. 6 and the thermal distribution developed from the results is further presented in Fig. 7.

Thermal states computed was exploited for estimating the effective plastic strain distribution. The maximum value of $\Delta\varepsilon p$ was detected on the solder layer, joining the frame and the silicon die. In particular, the most critical importance of the effective plastic strain was identified in correspondence of the solder layer corners. This is maybe due to the regular singularity. Fig. 7 (a) and (b) shows the effective plastic strain distribution in the proximity to the solder layer corner, where the highest value of εp was found in both thermal environmental conditions (T_c and T_h). This result well agrees with experimental evidence in literature obtained by Scanning Acoustic Microscope (SAM) observations developed on SMD devices and the number of cycles to failure for solder layer obtained for power cycle analysis is shown in Fig.7 (b). The crack propagation is nearly concentric, originating almost directly under the silicon chip that is the hottest point [41, 101].

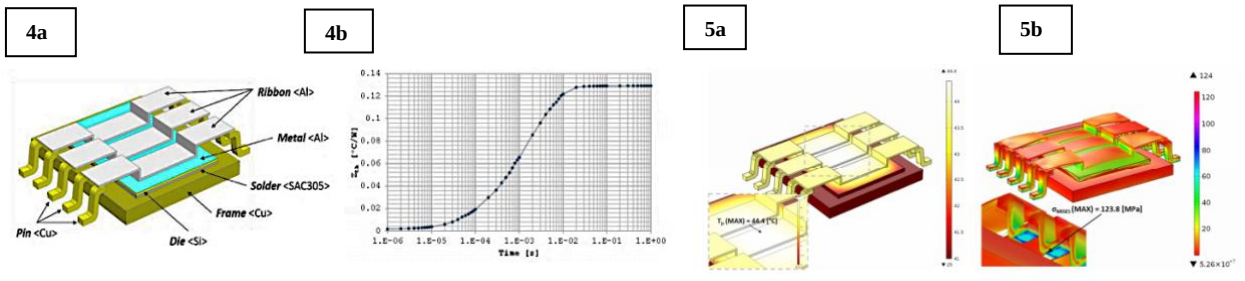

Figure 4: (a) Geometry of the numerical model (b) Effective plastic strain distribution for SAC305 solder die ($\boldsymbol{T_h} = 125$ [°C]); Figure 5: (a) Thermal map [°C] on the device and enlargement close to device central area (b)Von Mises stress distribution [MPa] in deformed configuration (50X) [41]

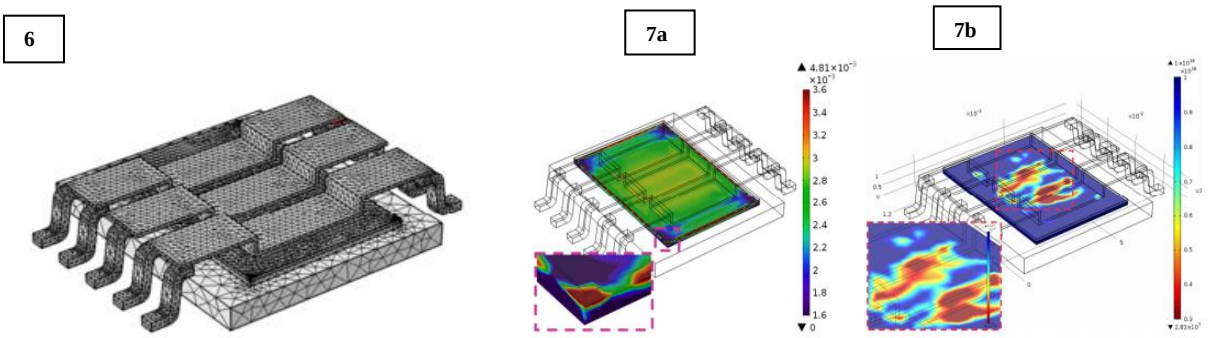

Figure 6: Computational mesh; Figure 7: (a) Effective plastic strain distribution for SAC305 solder, evaluated for T_h =125 [°C]; and enlargement close to solder corner (b) Number of cycles to failure for SAC305 solder die and enlargement close to central solder area [41].

The result of their investigations shows that the maximum von Mises stress calculated by the thermo-mechanical analysis is lower than the ultimate tensile strength (UTS) of materials. The fatigue life prediction results in excellent agreement with both the experimental and reviewed literature findings, both quantitatively (number of cycles to failure) and qualitatively (device portion subjected by the highest plastic strain). A comparative study of 14 different fatigue life prediction models is presented in Table 1 with their scope.

Table 1: Comparative Summary of Solder Joint Fatigue Models

Fatigue Model	Reference	Equation	Model Class	Coverage	Constant
Coffin Manson	[42]	$\frac{\Delta\varepsilon_p}{2} = \varepsilon_f(2N_f)^c$	Plastic strain	Low cycle fatigue	c = constant ε_f = fatigue ductility coefficier
Total Strain (Coffin Manson Basquin	[42]	$\frac{\Delta\varepsilon}{2} = \frac{\sigma_f}{E}(2N_f)^b + \varepsilon_f(2N_f)^c$	Plastic strain + elastic strain	High and low cycle fatigue	b = fatigue strength exponent c = fatigue ductility exponent ε_f = fatigue ductility coefficier σ_f = fatigue strength coefficier
Solomon	[43]	$\Delta\gamma_p N_p^{\alpha} = \theta$	Plastic shear strain	Low cycle fatigue	θ = fatigue ductility coefficient α = constant

Engelmaier	[44]	$N_f = \frac{1}{2}\left(\frac{\Delta\gamma}{2\varepsilon_f}\right)^{\frac{1}{c}}$	Total shear strain	Low cycle fatigue	$c = -0.442 - 0.0006T_{sj} + 0.0147\left(1 + \frac{360}{t_H}\right)$ f=cyclic frequency(cycles/day) $2\varepsilon_f = 0.65$ ε_f = fatigue ductility coefficien
Miner	[45]	$\frac{1}{N_f} = \frac{1}{N_p} + \frac{1}{N_c}$ $\frac{1}{N_f} = \frac{F_{pp}}{N_{pp}} + \frac{F_{cc}}{N_{cc}} + \frac{F_{cp}}{N_{cp}} + \frac{F_{pc}}{N_{pc}}$	Superposition (plastic and creep)	Plastic shear and matrix creep	N_p = plastic failure N_c = creep failure
Knecht and Fox	[46]	$N_f = \frac{C}{\Delta\gamma_{mc}}$	Matrix creep	Matrix creep only	N_f = Number of cycles to failure C = Constant $\Delta\gamma_{mc}$=Strain range due to matrix creep
Syed	[47]	$N_f = \frac{1}{(0.022D_{gbs} + 0.063D_{mc})}$	Accumulation of creep strain energy	Implies full coverage	D_{gbs} = accumulated equivalent creep strain/cycle D_{mc} = accumulated equivalent matrix creep/cycle
Dasgupta	[42]	$N_f = \left(\frac{\Delta\bar{W}_{total}}{W_0}\right)^{\frac{1}{k}}$	Total strain energy	Joint geometry accounted	$\Delta\bar{W}_{total}$ = total strain energy density, $W_0 = 0.1573$ $k = -0.6342$
Liang	[47]	$N_f = C(W_{ss})^{-m}$	Stress/strain energy density based	Constant from isothermal low cycle fatigue tests	C and m = temperature dependent material constants, W_{ss} = stress-strain hysteresis energy
Heinrich	[44, 45]	$N_0 = 18083\Delta W^{-1.46}$ $N_0 = 7860\Delta W^{-1.00}$	Energy density based	Hysteresis curve	ΔW = viscoplastic strain energy /cycle
Darveaux	[46]	$N_{aW} = N_{0s} + \frac{q - (N_{0s} - N_{0p})\frac{da_p}{dN}}{\frac{da_s}{dN} + \frac{da_p}{dN}}$	Energy density based	Hysteresis curve	a = total possible crack length, da = dN = crack growth, N_{0p} and N_{0s}= crack initiation energy-based terms
Pan	[47]	$C = N_f^*(a\dot{E}_p - b\dot{E}_c)$	Strain energy density	Hysteresis curve	C = strain energy density N_f^* = number of cycles to failure $\dot{E}_p$ = plastic strain energy density/cycle $\dot{E}_c$ = creep strain energy density/cycle
Stolkarts	[48]	$N_f = \frac{1 - (1 - d_f)^{k-1}}{(k+1)L}$	Damage accumulation	Hysteresis curve and damage evolution	k = material constant d = constant f =frequency
Noris and Landzberg	[49]	$AF = \frac{N_{field}}{N_{test}} = \left(\frac{f_{field}}{f_{test}}\right)^{-m}\left(\frac{\Delta T_{field}}{\Delta T_{test}}\right)^{-n}\left(e^{\frac{Ea}{k}\left(\frac{1}{T_{max,field}} - \frac{1}{T_{max,test}}\right)}\right)$	Temperature and frequency	Test condition versus use conditions	'field' and 'test' for use for field and test conditions respectively Ea = activation energy k = Boltzmann's constant $\frac{Ea}{k} = 1414$

Solder joints must maintain their mechanical and thermal integrity under various mechanical and thermal loads in service, including mechanical shock, thermal fatigue, creep, and mechanical shock. Mishandling of packages during manufacture, assembly, or by the user may cause solder joint failure. Because of the environmental concerns over the lead (Pb)-containing solders, lead-free solders, such as Sn-Ag-Cu (SAC) and Sn-Ag alloys, have been extensively utilised in electronic packaging. Fei et al. [50] examined the fracture of Sn-Rich (Pb-Free) solder joints under mechanical shock conditions.

The investigators used finite element analysis (FEA) to analyse the fracture behaviour of single solder joints by coupling void-induced solder-based fracture and IMC-controlled brittle fracture. To capture the influence of defects in the IMC, they modelled the IMC as an inhomogeneous material where material properties varies with location. They employed modified Gurson (GTN) model to simulate microvoid-induced ductile fracture. The GTN model proposes a yield surface given as:

$$\emptyset = \left(\frac{\sigma_e}{\sigma_y}\right)^2 + 2q_1 f \cos h\left(-\frac{3q_2}{2\sigma_y}\sigma_{kk}\right) - (1 + q_3 f^2) = 0 \quad (1)$$

Where f is void volume fraction and is defined as the volume of voids divided by the total volume of porous material (f = 0 describes an adequately dense material and, $f = 1$ signifies a wholly voided material); σ_y is the yield stress of the matrix material; q_1 is dependent on the strain-hardening behaviour of the metal, for example, $q_1 = 1.25$ for n = 20 and $q_1 = 1.8$ for n = 5, where n is the strain-hardening exponent. Recommendation shows that $q_2 = 1.0$ and $q_3 = q_1^2$. Fig. 8 shows representative yield surfaces expressed as the relationship between normalised von Mises effective stress and hydrostatic stress for $q_1 = 1.8$, $q_2 = 1.0$ and $q_3 = 3.24$. One can indisputably understand that the yield form differs on both the von Mises hydrostatic and effective stress and with increasing, void volume fraction, f, the material has the tendency to yield at diminutive von Mises and hydrostatic stress as shown in Fig. 9 (a) and (b) [51-53].

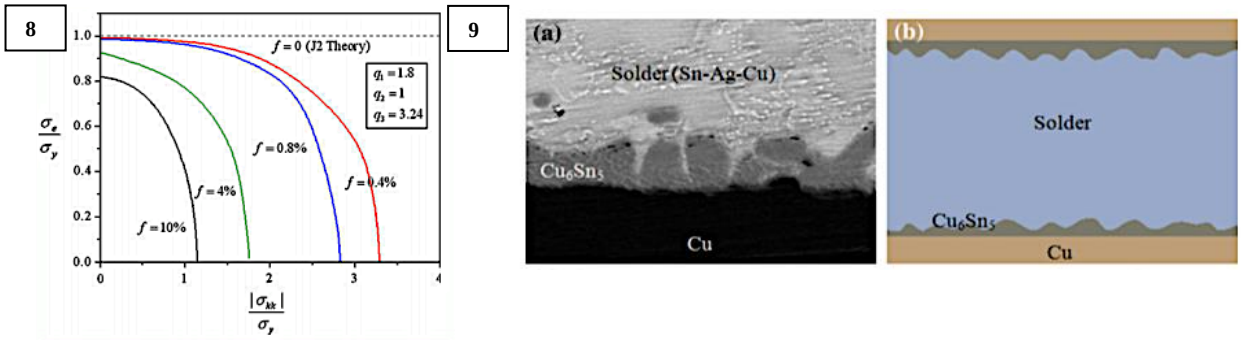

Figure 8: Schematic of the yield surface of the GTN model; both von Mises stress and hydrostatic stress affect the yield criterion; Figure 9: (a) Experimental image of a solder joint showing a nodule-shaped IMC. (b) Finite-element analysis model with a wavy-shape IMC/solder interface [51]

The outcome of their research demonstrates that the essential solder failure mechanism is dominated by fracture strength of solder and IMC growth. At reduced strain rates, the solder distorts plastically, and deformation in solder is constrained. At higher strain rates, the stress state is more triaxial. As the thickness of the IMC develops, defects in the IMC with pure fracture strength become more apparent, so that IMC-controlled fracture may happen. This outcome is furthermore usual at higher strain rates too. Consequently, the fracture of the solder joint depends on both IMC thickness and strain rate. In describing the qualitative mechanism of solder joint fracture, a "mechanism chart" of solder joint fracture recommended is shown in Fig. 10. The fracture strength of solder rises with strain rate (Fig. 10a), while that of IMC reduces with IMC thickness (Fig. 10b). The connection between the fracture strength of solder and IMC forms the crucial state for solder joint fracture (Fig. 10c). The prognosis of the connection line is presented in the IMC thickness/strain rate space (Fig. 10d). The line divides the IMC-controlled fracture (brittle) and solder-controlled fracture (ductile).

Tang et al. [54] investigated the FEA of SAC solder joint failure under impact test. They used a physical model of ball impact test (μm) shown in Fig. 11 (a) and the FEM half-symmetry is shown in Fig. 11 (b). In their research, they applied ANSYS LS-DYNA for the structural response of solder joints under high-speed impact test. Mathematical simulation outcomes show that three kinds of failure modes in ball impact test are simulated based on tiebreak connection established model design. They concluded that the fracture time grows with an increase of IMC strength. Failure time utilised was 30μs for a brittle break, 40μs~100μs for a medial break and above 100μs for a ductile break

respectively. The maximum shear force is between 1.3N to 13N, which is significantly lower than the original impact force, owing to the neglect of the hardening mechanism of material constrained to high strain ratio loading.

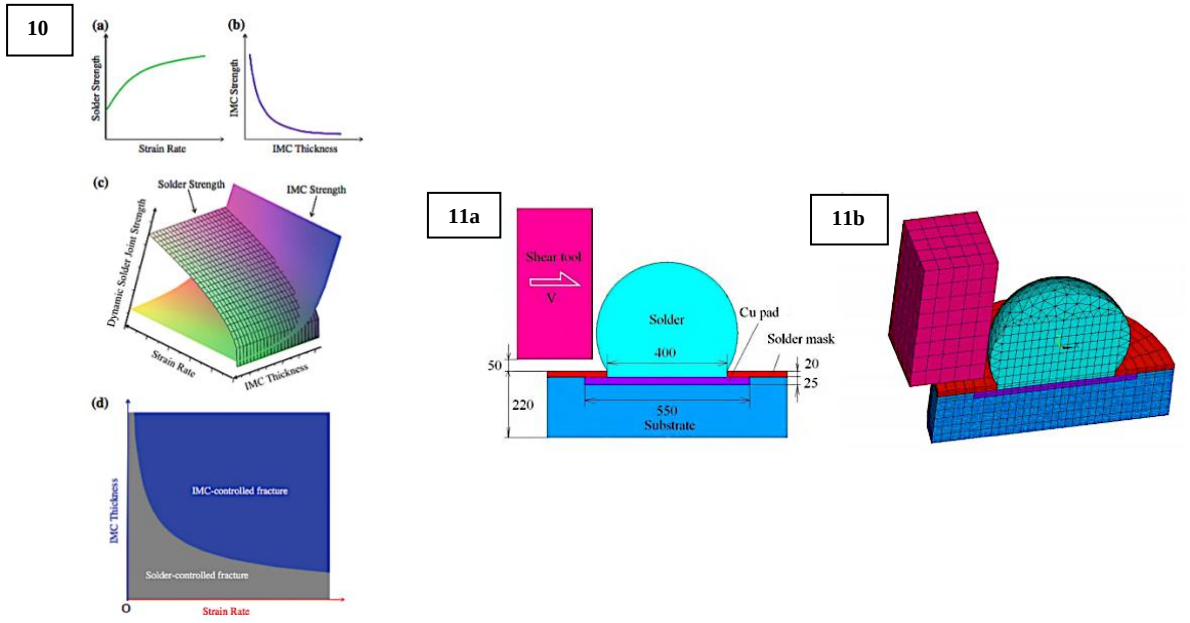

Figure 10: (a) Fracture strength of solder increases with strain rate. (b) Fracture strength of IMC decreases with IMC thickness. (c) The 3-D relation is coupling the IMC thickness effect and applied strain rate effect together. (d) Solder-controlled and IMC-controlled; Figure 11: (a) Physical model of ball impact test (units: μm) (b) Half-symmetry of Finite Element Model (FEM) [54]

2.2 Fatigue life prediction of solder joints

Fatigue damage is a serious concern in engineering applications involving cyclic or repetitive loading and can lead to fracture and catastrophic failure of materials and resources. Avoiding or somewhat delaying the failure of any electronic component exposed to cyclic loading is the ultimate goal of engineers or researchers who are involved in electronic system design and development. Packaging in electronics devices comprises of materials with very different mechanical and thermal properties. In service, discrepancies of CTE of various materials produces cycling shear stress on solder joints. The stresses build fatigue failure of solder joints, and fatigue life of solder joints typically determines the reliability of electronic packaging. Thus, the prediction of fatigue life is an important step in the design and development of electronic products [55, 56].

The mathematical models that are used for predicting fatigue life are comprised of two groups. The first group is made up of models based on the prediction of crack nucleation, using a combination of damage evolution rule and criteria based on stress/strain of components. One of the essential characteristics of these models is the absence of dependence from loading and specimen geometry, being the fatigue life defined only by a stress/strain model [57, 58]. The method of the second group is based alternatively on continuum damage mechanics (CDM), in which fatigue life is predicted by measuring a damage parameter, cycle by cycle. Ordinarily, the life prediction of elements subjected to fatigue is based on the "safe-life" methodology [59, 60], coupled with the rules of linear cumulative damage [61, 62].

Paris & Erdogan formulated a power law which is commonly used to model stable fatigue crack growth [63]:

$$\frac{da}{dN} = C * \Delta K^m \quad (2)$$

Moreover, the fatigue life *N* obtainable from the following integrated equation:

$$N = \int_{a_i}^{a_f} \frac{da}{C*\Delta K^{m'}} \quad (3)$$

Where the stress intensity factor range is represented by ΔK, and C and m are the material-related constants. The integration limits a_f and a_i represents the initial and final fatigue crack lengths; the crack propagation theory expressed as:

$$\frac{da}{dN} = C' * \Delta J^{m'} \quad (4)$$

Where ΔJ is the J integral range corresponding to equation 16, while C' and m' are constants [62-65].

2.3 Isothermal fatigue of solder joints

Wiese et al. investigated the fracture behaviour of flip chip solder joints. Their research examined Sn63Pb37 and Sn95.5Ag4.0Cu0.5 solder materials with a test temperature of 300K. The strain wave amplitudes ranged from $\Delta\varepsilon$ = 0.3 % ... 4.0% and the strain wave frequencies ranged from f = 0.0004 Hz ... 10 Hz. A flip chip specimen is shown in Fig. 12 [66].

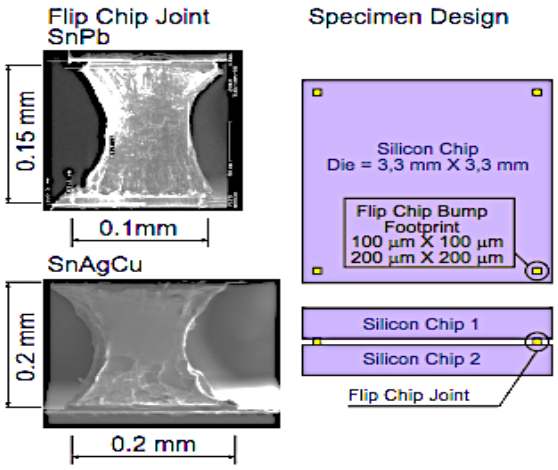

Figure 12: Flip Chip Specimen [66]

The crack propagation rate is calculated by:

$$\frac{da}{dN} = \sqrt{n * d^2 * -\frac{d\Delta F}{dN} * \frac{1}{\Delta F_0}} \quad (5)$$

Where n is the number of cracks that grow spherical and d is the diameter of the joint at the section where the crack propagates: The parameter ΔF corresponds to the force amplitude at the current cycle, while ΔF_0 represents the force amplitude at the initial cycle. Guo & Conrad [67] introduced a power law that correlated the crack growth rate da/dN with the plastic strain energy (ΔW_{pl}) as:

$$\frac{da}{dN} = \alpha * (\Delta W_{pl})^{\beta} \quad (6)$$

For accumulated inelastic strain (ε_{acc}):

$$\frac{da}{dN} = \alpha * (\varepsilon_{acc})^{\beta} \quad (7)$$

Zhang et al. [68] investigated the isothermal mechanical durability of three selected PB-free solders: Sn3.9Ag0.6Cu, Sn3.5Ag, and Sn0.7Cu. They used specimens comprising of two copper plates joined in a lap configuration by a thin layer of solder to characterise the isothermal mechanical durability of three lead-free solders (Sn-3.9Ag-0.6Cu, Sn-3.5Ag, and Sn-0.7Cu) and compared with those of the eutectic Sn-37Pb solder at the room temperature and at 135°C. The Sn-3.9Ag-0.6Cu and Sn-3.5Ag had much better durability than the Sn- 37Pb, but the Sn-0.7Cu was worse. They used the Morrow energy model (equation 30), which links fatigue life ($\mathbf{N_f}$) with plastic strain energy density ΔW. The results of their report can be used for virtual qualification of Pb-free electronics during the design and development of electronics under mechanical loading.

$$\mathbf{N_f^m \Delta W = C} \tag{8}$$

CTE mismatch is the common problem of fatigue failure that occurs from cyclic loading. A model of the linear CTE mismatch is provided by the difference in the linear coefficient of thermal expansion of the contacting materials, the physical length of the component and the difference in temperature, expressed by:

$$\mathbf{D_u = \Delta e \cdot L \cdot \Delta T} \tag{9}$$

Where D_u is a thermal mismatch; Δe is the difference in CTE between the materials; L is the linear dimension of the component, and ΔT is the temperature changed. In reducing solder joint cracks, it is essential to reduce the thermal mismatch, which can be done by limiting the difference in CTE, minimising the temperature delta or reducing the size of the component. For high reliability, any mismatch of CTE must be supported by the solder joint [54, 69-70]. Fig 13 shows solder joints subjected to shear loading due to CTE mismatch.

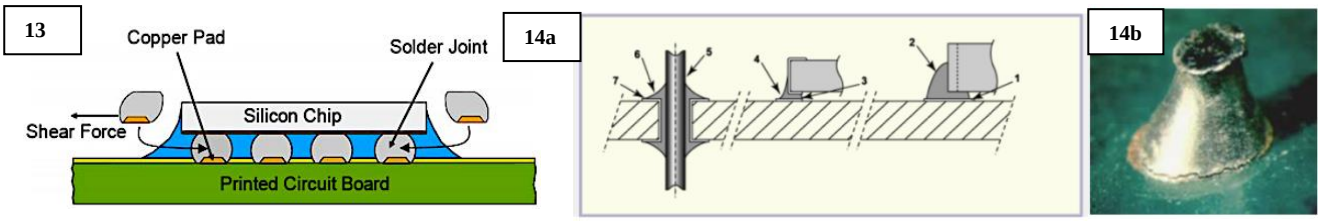

Figure 13: Solder joints subjected to shear loading due to CTE mismatch; Figure 14: (a) Fatigue susceptible locations in solder joints and (b) Cracked through-hole joint [72]

Their result concluded that the CTE evolution of lead-free solder could be explained by the microstructural changes in the solder alloys during isothermal ageing. Thermal ageing induces the coarsening of different phases of the solder, resulting in a higher coefficient of thermal expansion. In contrast, the addition of microalloying elements into the solder alloys impedes the CTE developments with ageing. CTE evolution during isothermal ageing recommends potential reliability difficulties for lead-free solder joints subjected to long-term exposures to severe temperatures. The parts where cracks will become noticeable under thermal cycling environments are shown in Fig. 14 (a) by the numbers 1 to 7 and 14 (b) shows cracked through-hole joint [71-72]. Coupled with the CTE mismatch connecting different elements of the device, cyclic thermal loading results in stress reversals and possible growth of inelastic strain in the solder joint. This inelastic strain grows with repeated cycling and eventually produces solder joint cracking and interconnection failures [48, 97]

For lead-free materials/devices:

1) At the interface connecting solder and metallisation under significant components such as lead-free chip carriers.
2) At the vertical interface between the end metallisation and solder fillet of SM devices.

3) At the interface between foil and solder under chip components such as resistors and multilayer capacitors.
4) In the bulk solder portion of the solder joint fillet.

For through-hole materials/devices:

5) Annular cracks at the interface within solder fillet and wire.
6) In the majority of the fillet.
7) Between joint and pad.

3.0 Creep Failure of Solder Joints

The long-term reliability of solder joint is a fundamental necessity for electronics packaging. Solder joint failure, nonetheless, can comprise of compound mechanisms. One of the various simple failure processes in metals/alloys is the creep phenomenon. Creep is described as a time-dependent deformation when a material is subjected to stress for an extended period. This time-dependent deformation can hypothetically happen at any temperature over the absolute zero. Nevertheless, creep-dominant failure conventionally appears under elevated temperature close to the melting point of the material. Lead-free solders are low-temperature alloys with a melting point or liquidus/solidus temperature in the range of 210 – 230°C. Subsequently, a detectable creep process under low level of mechanical load is expected even at ambient temperature. The research by Hwang & Vargas [72] shows that the initial data on the relative creep rate of twenty-two common solder alloys and endeavours to correlate the creep rate to the melting point, tensile strength, modulus, microstructure of alloys. The alloys under analysis comprises of Sn/Sb, Sn/Pb/Bi, Sn/Pb/Sb, Sn/Bi, Sn/In, Sn/Pb, Sn/Pb/Ag, Sn/Ag and Pb/in systems. They also examined the recommended mechanisms for solder creep phenomena.

Lee et al. [73] investigated the mechanisms of creep deformation in pure Sn solder joints. The work reported by the investigators involves the creep of pure Sn solder joints with Cu metallization (Cu||Sn||Cu). The steady-state creep tests in shear are connected with electron backscatter diffraction (EBSD) investigation of the evolution of the microstructure during creep to define the deformation mechanism and the characteristics of the microstructural development. The creep behaviour of the joint changes significantly with temperature. The results imply that a “segmented” constitutive equation of Dorn type is most suitable for the low-temperature behaviour, while a “hyperbolic” constitutive equation preferably at high temperature. Related work was undertaken by Lee et al. [74, 77], Weertman [75] and Herring [76]. Weertman [75] and Wong et al. [78] examined the creep-fatigue models of solder joints. They reviewed creep-fatigue models in the aerospace and power electronics. Although the investigation by Choudhury et al. [79] identified a new SAC alloy with better thermal and mechanical reliability than Sn-Ag3-Cu0.5/Sn-Ag4-Cu0.5, research has not adequately studied the creep failure. Creep properties at high temperature give an excellent indication of the thermal cycling performance of the solder alloy. This is necessary throughout alloy advancement because thermal cycling testing demands time and needs resources such as supply of power during experimentation.

3.1 Solder Alloy Creep Model

As far as joining material concerned, solder alloys are widely used in all electronic packaging due to their lower melting temperature and excellent wetting properties. However, in most electronic packaging, solder alloys function at the thermally activated condition at room temperature, as a result of their low melting point. Numerous thermally activated developments, including grain boundary diffusion, dislocation-glide, dislocation climb, and lattice diffusion generate and accrue an enormous quantity of creep deformations [73, 80]. These resulted in different kinds of failures in electronic

packaging, particularly in soldered joints. Only a limited number of creep models are developed for viscoplastic behaviours of solder joints. Lee & Basaran [73], Gomez & Basaran [80] and Basaran et al. [81] have listed these references comprehensively on constitutive modelling of solder alloys. The analyses have shown that the creep behaviour of a solder alloy significantly depends on age, stress, temperature, and grain size. However, a full review and an evaluation of these models have never been published.

Zhu et al. [82] suggested a new life prediction model under high strain rate with the experimental result compared with the predicted outcome and showed that the calculation life meets well with the test life under high strain rate. Ramachandran & Chiang [83] used unified viscoplastic Anand model to describe the rate-dependent behaviour of both eutectic and lead-free solder alloys at high homologous temperatures. The most regularly used creep model denotes the effect of grain size and stress exponent term and, the shear stress and shear modulus characterise it.

Kashyap & Murty [84] and Hacke et al. [85] has recommended that this is the best universally used creep model is called Model 1 as shown in equation 10:

$$\text{Model 1:}\quad \dot{\boldsymbol{\gamma}} = \left(\mathbf{A}\frac{\mathbf{Gb}}{\mathbf{kT}}\right)\left(\frac{\mathbf{b}}{\mathbf{d}}\right)^{\mathbf{p}}\left(\frac{\boldsymbol{\tau}}{\mathbf{G}}\right)^{\mathbf{n}}\left[\mathbf{D_o}\mathbf{exp}\left(-\frac{\mathbf{Q}}{\mathbf{RT}}\right)\right] \tag{10}$$

where $\dot{\gamma}$ is a creep strain rate; A is a material constant; G is the shear modulus; b is the burger's vector; k is the Boltzmann's constant; T is the absolute temperature; d is the grain size, τ is the applied shear stress; n is the stress coefficient; Q is the activation energy for creep process, and R is a universal constant. The Anand model which was proposed by Anand is shown in equation 11 [86, 87].

$$\dot{\boldsymbol{\varepsilon}}^{\mathbf{in}} = \mathbf{A}\left[\mathbf{sinh}\left(\boldsymbol{\xi}\frac{\boldsymbol{\sigma}}{\mathbf{s}}\right)\right]^{\frac{\mathbf{1}}{\mathbf{m}}}\mathbf{exp}\left(-\frac{\mathbf{Q}}{\mathbf{RT}}\right) \tag{11}$$

where $\dot{\varepsilon}^{in}$ is the inelastic strain rate, ξ is a multiplier of stress, σ is the applied stress, s is a single scalar as an internal variable to represent the average isotropic resistance to plastic flow, and m is the strain rate sensitivity of stress. A steady-state creep equation is obtained by simplifying Anand Model. Model 2 is obtained as seen in equation 12:

$$\text{Model 2:}\quad \dot{\boldsymbol{\gamma}} = \mathbf{A}(\mathbf{sinh}\boldsymbol{\beta}\boldsymbol{\tau})^{\mathbf{n}}\mathbf{exp}\left(-\frac{\mathbf{Q}}{\mathbf{RT}}\right) \tag{12}$$

Where n is $\frac{1}{m}$, and β is the multiplier of hyperbolic-sine law obtainable from curve fitting to experimental data with the use of linear and non-linear least squares regression. Pan proposed the modification of the Anand model. Model 3 possesses additional grain size as well as some term original embedded into Model 2 as seen in equation 13 [88]:

$$\text{Model 3:}\quad \dot{\gamma} = A(\sinh\beta\tau)^{n}(d)^{-p}\exp\left(-\frac{Q}{RT}\right) \tag{13}$$

A creep function Model 4 was recommended by Darveaux& Banerji [89] as seen in equation 14. It is similar to Model 2:

$$\text{Model 4:}\quad \dot{\boldsymbol{\gamma}} = \mathbf{A}\left(\frac{\mathbf{G}}{\mathbf{T}}\right)\left(\mathbf{sinh}\boldsymbol{\beta}\frac{\boldsymbol{\tau}}{\mathbf{G}}\right)^{\mathbf{n}}\mathbf{exp}\left(-\frac{\mathbf{Q}}{\mathbf{RT}}\right) \tag{14}$$

Another valuable creep model 'Model 5' was recommended by Shi et al. [90], Model 5 is shown in equation 15. The model presumed that there are two systems of steady-state creep and that individual

regime has a power law dependence on stress and strain rate. Shi et al. [90] also recommended another Model 6 in equation 16 founded on their experimental outcomes.

Model 5: $$\dot{\boldsymbol{\gamma}} = \mathbf{A_1}\left(\frac{\boldsymbol{\tau}}{\mathbf{G}}\right)^{\mathbf{n_1}} \mathbf{exp}\left(-\frac{\mathbf{Q_1}}{\mathbf{RT}}\right) + \mathbf{A_2}\left(\frac{\boldsymbol{\tau}}{\mathbf{G}}\right)^{\mathbf{n_2}} \mathbf{exp}\left(-\frac{\mathbf{Q_2}}{\mathbf{RT}}\right) \quad (15)$$

Model 6: $$\dot{\boldsymbol{\gamma}} = \mathbf{A_1}\left(\frac{\mathbf{G}}{\mathbf{T}}\right)\left(\mathbf{sinh}\boldsymbol{\beta}\frac{\boldsymbol{\tau}}{\mathbf{G}}\right)^{\mathbf{n_1}} \mathbf{exp}\left(-\frac{\mathbf{Q_1}}{\mathbf{RT}}\right) + \mathbf{A_2}\left(\frac{\mathbf{G}}{\mathbf{T}}\right)\left(\mathbf{sinh}\boldsymbol{\beta}\frac{\boldsymbol{\tau}}{\mathbf{G}}\right)^{\mathbf{n_2}} \mathbf{exp}\left(-\frac{\mathbf{Q_2}}{\mathbf{RT}}\right) \quad (16)$$

Lee & Basaran [89] proposed a modify Anand model considering, shear modulus temperature dependency and grain size for Model 7 and 8 as shown in equation 17 & 18:

Model 7: $$\dot{\boldsymbol{\gamma}} = \mathbf{A}\left(\mathbf{sinh}\boldsymbol{\beta}\frac{\boldsymbol{\tau}}{\mathbf{G}}\right)^{\mathbf{n}} \mathbf{exp}\left(-\frac{\mathbf{Q}}{\mathbf{RT}}\right) \quad (17)$$

Model 8: $$\dot{\boldsymbol{\gamma}} = \mathbf{A}\left(\frac{\mathbf{b}}{\mathbf{d}}\right)^{\mathbf{p}}\left(\mathbf{sinh}\boldsymbol{\beta}\frac{\boldsymbol{\tau}}{\mathbf{G}}\right)^{\mathbf{n}} \mathbf{exp}\left(-\frac{\mathbf{Q}}{\mathbf{RT}}\right) \quad (18)$$

A hyperbolic-sine term was utilised instead of power-law used in Dorm equation given in Model 1. When Model 7 was compared with Model 8, they suggested an observation of the effect of Gb/kT. Model 9 was discovered in equation 19:

Model 9: $$\dot{\boldsymbol{\gamma}} = \mathbf{A}\left(\frac{\mathbf{Gb}}{\mathbf{kT}}\right)\left(\frac{\mathbf{b}}{\mathbf{d}}\right)^{\mathbf{p}}\left(\mathbf{sinh}\boldsymbol{\beta}\frac{\boldsymbol{\tau}}{\mathbf{G}}\right)^{\mathbf{n}} \mathbf{exp}\left(-\frac{\mathbf{Q}}{\mathbf{RT}}\right) \quad (19)$$

The findings by Lee & Basaran [89] and Shi et al. [90] concluded that creep laws with the τ/G term in overall yield better results than those of stress term only represented by shear stress, τ and that grain size also plays an important role that cannot be ignored in creep model. Creep laws given in model 7, 8 and 9 were the most successful for experimental data. The differential form of the evolution equation for the internal variable s is assumed to be in the form:

$$\dot{\mathbf{s}} = \mathbf{h}(\boldsymbol{\sigma}, \mathbf{s}, \mathbf{T})\dot{\boldsymbol{\varepsilon}}_{\mathbf{p}} \quad (20)$$

$$\dot{\mathbf{s}} = \left[\mathbf{h_o}\left(\mathbf{1} - \frac{\mathbf{s}}{\mathbf{s}^*}\right)^{\mathbf{a}} \mathbf{sigh}\left(\mathbf{1} - \frac{\mathbf{s}}{\mathbf{s}^*}\right)\right]\dot{\boldsymbol{\varepsilon}}_{\mathbf{p}}; \mathbf{a} > \mathbf{1} \quad (21)$$

Where $h(\sigma, s, T)$ is associated with the recovery process and progressive hardening. Parameter h_o is the hardening constant, a is the strain rate sensitivity of the hardening process, and the term s^* is expressed as:

$$\mathbf{s}^* = \hat{\mathbf{s}}\left[\frac{\dot{\boldsymbol{\varepsilon}}_{\mathbf{p}}}{\mathbf{A}}\mathbf{e}^{\left(\frac{\mathbf{Q}}{\mathbf{RT}}\right)}\right]^{\mathbf{n}} \quad (22)$$

Where $\hat{s}$ is a coefficient and n is the strain rate sensitivity of the saturation value deformation resistance: For $s < s^*$, equation 16 can be written as:

$$\mathbf{ds} = \mathbf{h_o}\left(\mathbf{1} - \frac{\mathbf{s}}{\mathbf{s}^*}\right)^{\mathbf{a}} \mathbf{d}\boldsymbol{\varepsilon}_{\mathbf{p}} \quad (23)$$

moreover, then integrated to yield

$$\mathbf{s} = \mathbf{s}^* - \left[(\mathbf{s}^* - \mathbf{s_o})^{\mathbf{1-a}} + (\mathbf{a} - \mathbf{1})\{(\mathbf{h_o})(\mathbf{s}^*)^{-\mathbf{a}}\}\boldsymbol{\varepsilon}_{\mathbf{p}}\right]^{\frac{\mathbf{1}}{\mathbf{1-a}}} \quad (24)$$

Where $s(0) = s_o$ represents the initial value of s at the time, $t = 0$. Substituting equation 22 into equation 24 yields version of evolution equation for the internal variable s:

$$\mathbf{s} = \hat{\mathbf{s}}\left[\frac{\dot{\boldsymbol{\varepsilon}}_\mathbf{p}}{\mathbf{A}}\mathbf{e}^{\left(\frac{\mathbf{Q}}{\mathbf{RT}}\right)}\right]^{\mathbf{n}} - \left[\left(\hat{\mathbf{s}}\left[\frac{\dot{\boldsymbol{\varepsilon}}_\mathbf{p}}{\mathbf{A}}\mathbf{e}^{\left(\frac{\mathbf{Q}}{\mathbf{RT}}\right)}\right]^{\mathbf{n}} - \mathbf{s_o}\right)^{(\mathbf{1-a})} + (\mathbf{a-1})\left\{(\mathbf{h_o})\left(\hat{\mathbf{s}}\left[\frac{\dot{\boldsymbol{\varepsilon}}_\mathbf{p}}{\mathbf{A}}\mathbf{e}^{\left(\frac{\mathbf{Q}}{\mathbf{RT}}\right)}\right]^{\mathbf{n}}\right)^{-\mathbf{a}}\right\}\boldsymbol{\varepsilon}_\mathbf{p}\right]^{\frac{\mathbf{1}}{\mathbf{1-a}}} \quad (25)$$

or

$$\mathbf{s} = \mathbf{s}^*\left(\dot{\boldsymbol{\varepsilon}}_\mathbf{p}, \boldsymbol{\varepsilon}_\mathbf{p}\right)$$

The final Anand model equation is the stress equation, the flow equation, and the integrated evolution equation above. The material parameters, A, Q/RT, m ,h_o, a, s_o, ŝ and n are constants [85, 91]. The post-yield uniaxial stress-strain relations predicted by the Anand model are acquired by substituting the expression for internal variable s from equation 17 above into the stress, σ shown in equation 24:

$$\boldsymbol{\sigma} = \frac{\mathbf{s}}{\boldsymbol{\xi}}\mathbf{sinh}^{-\mathbf{1}}\left\{\left[\frac{\dot{\boldsymbol{\varepsilon}}_\mathbf{p}}{\mathbf{A}}\mathbf{e}^{\left(\frac{\mathbf{Q}}{\mathbf{RT}}\right)}\right]^{\mathbf{m}}\right\} \quad (26)$$

The calculation results in:

$$\boldsymbol{\sigma} = \frac{\mathbf{1}}{\boldsymbol{\xi}}\mathbf{sinh}^{-\mathbf{1}}\left\{\left[\frac{\dot{\boldsymbol{\varepsilon}}_\mathbf{p}}{\mathbf{A}}\mathbf{e}^{\left(\frac{\mathbf{Q}}{\mathbf{RT}}\right)}\right]^{\mathbf{m}}\right\}\left(\hat{\mathbf{s}}\left[\frac{\dot{\boldsymbol{\varepsilon}}_\mathbf{p}}{\mathbf{A}}\mathbf{e}^{\left(\frac{\mathbf{Q}}{\mathbf{RT}}\right)}\right]^{\mathbf{n}} - \left[\left(\hat{\mathbf{s}}\left[\frac{\dot{\boldsymbol{\varepsilon}}_\mathbf{p}}{\mathbf{A}}\mathbf{e}^{\left(\frac{\mathbf{Q}}{\mathbf{RT}}\right)}\right]^{\mathbf{n}} - \mathbf{s_o}\right)^{(\mathbf{1-a})} + (\mathbf{a-1})\left\{(\mathbf{h_o})\left(\hat{\mathbf{s}}\left[\frac{\dot{\boldsymbol{\varepsilon}}_\mathbf{p}}{\mathbf{A}}\mathbf{e}^{\left(\frac{\mathbf{Q}}{\mathbf{RT}}\right)}\right]^{\mathbf{n}}\right)^{-\mathbf{a}}\right\}\boldsymbol{\varepsilon}_\mathbf{p}\right]^{\frac{\mathbf{1}}{\mathbf{1-a}}}\right) \quad (27)$$

or

$$\boldsymbol{\sigma} = \boldsymbol{\sigma}^*(\dot{\boldsymbol{\varepsilon}}_\mathbf{p}, \boldsymbol{\varepsilon}_\mathbf{p}) \quad (28)$$

For the UTS, this can be obtained from the equation above. The UTS is given by the limit as $\varepsilon_p \rightarrow \infty$:

$$\text{UTS} = \boldsymbol{\sigma}|\boldsymbol{\varepsilon}_\mathbf{p} \rightarrow \infty| = \frac{\hat{\mathbf{s}}}{\boldsymbol{\xi}}\left[\frac{\dot{\boldsymbol{\varepsilon}}_\mathbf{p}}{\mathbf{A}}\mathbf{e}^{\left(\frac{\mathbf{Q}}{\mathbf{RT}}\right)}\right]^{\mathbf{n}}\mathbf{sinh}^{-\mathbf{1}}\left\{\left[\frac{\dot{\boldsymbol{\varepsilon}}_\mathbf{p}}{\mathbf{A}}\mathbf{e}^{\left(\frac{\mathbf{Q}}{\mathbf{RT}}\right)}\right]^{\mathbf{m}}\right\} = \boldsymbol{\sigma}^* \quad (29)$$

When yield stress is given by the limit $\varepsilon_p \rightarrow 0$

$$\sigma_Y = \sigma|\varepsilon_p \rightarrow \infty| = cs_0 = \frac{1}{\xi}\sinh^{-1}\left\{\left[\frac{\dot{\varepsilon}_p}{A}e^{\left(\frac{Q}{RT}\right)}\right]^m\right\}s_0 = \sigma_0 \quad (30)$$

Using saturation stress, $\boldsymbol{\sigma}^* = \mathbf{UTS}$ relation above, the post-yield stress-strain response (power law) equation 30 above can be rewritten as:

$$\sigma = \sigma^* - \left[(\sigma^* - cs_0)^{(1-a)} + (a-1)\{(ch_0)(\sigma^*)^{-a}\}\varepsilon_p\right]^{\frac{1}{(1-a)}} \quad (31)$$

4.0 Combined effect of creep and fatigue

The mechanisms associated when creep and fatigue act together are inadequately understood, but there is an indication that the summation of their properties is even more important than their distinctive influences. Since solders function at elevated homologous temperatures, if they have small stress acting on them, they are economically creeping all the time. Therefore, any methodology of stress or thermal cycling will present an unwanted occurrence of the combined effect of creep and fatigue. To make the circumstances worse, duty cycles could be:

1. Fluctuating stress levels at a constant high homologous temperature.
2. Fluctuating elevated homologous temperatures under constant stress.
3. Concurrent fluctuations in high homologous temperature and stress.
4. Any sequence of 1, 2 or 3.

According to the research conducted by Huang et al. [92], it was acknowledged that SAC305 lead-free solder joint presents an excellent thermostable performance. Failures of the lead-free solder joint were studied under thermal cycling and thermal ageing conditions. The crack initiation point was found to have developed in the bulk solder and propagated along the IMC. The location of fracture is primarily around the interface between the IMC layers and solder joint, and moreover, this may happen in the solder near the pad. After a specific time of observing the thermal cycling test, the spreading trend of the crack is shown and, the crack of the solder joint slowly changed from one crack to two or more cracks and the length become extended [93, 94]. With the increased rate of the thermal cycling, the cracks continued along the IMC [95, 96].

5.0 Finite Element Modelling

Generally, finite element method consists of three stages: (1) pre-processing, where the analyst generates the finite element mesh and applies specific parameters or boundaries to the model, (2) solver/solution, where the program runs the governing mathematical equation that was produced by the model and (3) post-processing, where the outcome is assessed and verified for additional analysis. Karayan et al. [97], Borst & Sluys [98] and Ortiz et al. [99] research give an example of a mechanical failure analysis assessment that used finite element analysis software to verify findings regarding the failure incidents. Half 3D model was developed according to the original ball joint test samples as shown in Fig. 11(a). After modelling, linear hexahedral solid elements are administered except the outer region of the solder joint where anticipation of force concentration and large deformation illustrates. Alternatively, linear tetrahedral elements are applied for a further detailed simulation as presented in Fig. 15 – 17 [54]. Automatic nodes-to-surface contact is applied to the shear tool and solder ball, during tiebreak nodes-to surface contact between the solder and Cu pad. Tiebreak contact links adjacent meshes and limits the movements of nodes till the bond force is surpassed; the bond failure is characterised by:

$$\left(\frac{|\mathbf{f_s}|}{\mathbf{S_n}}\right)^{\mathbf{2}} + \left(\frac{|\mathbf{f_s}|}{\mathbf{S_s}}\right)^{\mathbf{2}} \geq \mathbf{1} \tag{32}$$

Where the subscripts n and s denote normal, and shear, respectively, and f and S is the calculated nodal force and the given ultimate nodal force at which the bond breaks respectively. The stress distribution in failure Model 1, 2 and 3 as shown in Fig. 15, 16 & 17. For Model 1, Fig. 15, the interfacial fracture takes place within 45μs, and the solder bump is sheared off by the shear tool. Model 2, Fig. 16 shows much more IMC strength (500MPa and above), solder surfers higher stress throughout the shear impact procedure. Fracture originates at 33μs on the left edge of the interface till 60μs while solder bulk starts to fail as a result of an overload of shear force and Model 3, Fig. 17 indicate that the IMC strength is too high to break that failure only occurs in the solder. The interrelating period between the shear tool and solder is comparatively longer. Even after 132μs, half of the ball is remaining on the pad [54, 100].

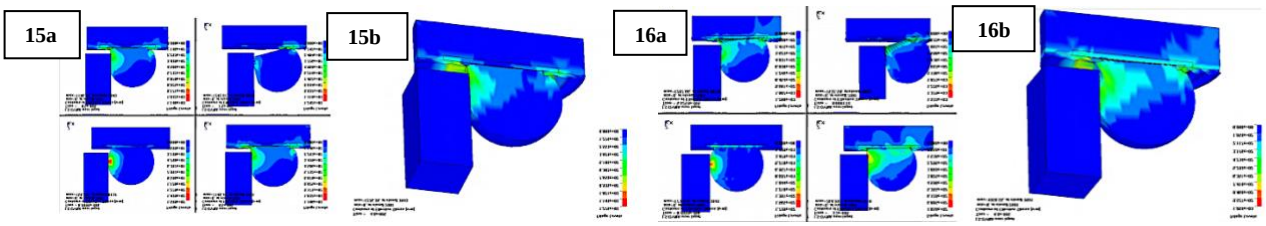

Figure 15: (a) Animations of failure Model 1 (b) Stress distribution in the entire mode; Figure 16: (a) Animations of failure Model 2 (b) Stress distribution in the entire mode [54]

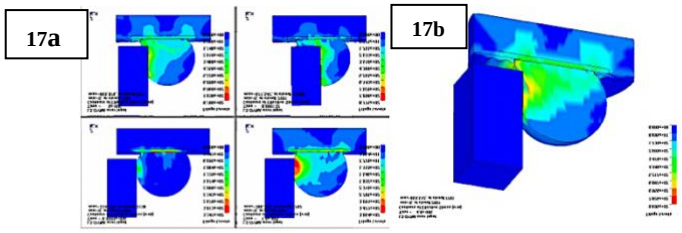

Figure 17: a) Animations of failure Model 3 (b) Stress distribution in the entire mode [54]

6.0 Summary

Advancement in failure studies of the solder joint, in particular fatigue and creep has been examined. The dominant mechanisms responsible for effecting the solder damage for predicting the fatigue lives of solder joints failures is by stress, strain, energy and damage-accumulation. Any other fatigue model that fit none of the above categories is usually empirically based. Although there are various models used by numerous researchers, few models such as the Coffin-Manson model (plastic strain), Miner Cumulative Damage model (plastic and creep strain) which combines Solomon's fatigue model with Knecht's and Fox's creep model and Dasgupta model based on energy are used mostly by researchers because it captures the different and fundamental fatigue failures modes of a solder joint. For creep-strain fatigue failure, Darveaux model of inelastic strain rate is typically used for verifying creep failures. The paper summarises the mathematical models used to define fatigue and creep failures. Although several mathematical models are proposed to individually address creep and fatigue deformations, no such models currently exist that can adequately simulate the combined effect of creep and fatigue deformations. Thus, there is the need for further research to investigate the process of solder joint failures that focuses on modelling (simulation) of both fatigue and creep failures.

Acknowledgement

The authors gratefully acknowledge the PhD funding contributions of University of Derby.

References

[1] S. Ahmed, M. Basit, J. C. Suhling and P. Lall, "Effects of ageing on SAC-Bi solder materials," in 2016 15th IEEE Intersociety Conference on Thermal and Thermomechanical Phenomena in Electronic Systems (ITherm), Las Vegas, NV, 2016.

[2] J. Zhang, Z. Hai, S. Thirugnanasambandam, J. L. Evans, M. J. Bozack, R. Sesek, Y. Zhang and J. C. Suhling, "Correlation of Aging Effects on Creep Rate and Reliability in Lead Free Solder Joints," SMTA Journal, vol. 25, no. 3, pp. 19-28, 2010.

[3] E. H. Amalu, "Modelling of the Reliability of Flip Chip Lead-Free Solder Joints at High-Temperature excursions," Amalu, Emeka Hyginus, Medway, Kent, 2012.

[4] K. Kanlayasiri and K. Sukpimai, "Effects of indium on the intermetallic layer between low-Ag SAC0307-xIn lead-free solders and Cu substrate," Journal of Alloys and Compounds, vol. 668, pp. 169-175, 2016.

[5] L. Zhang and K. Tu, "Materials Science & Engineering," Structure and properties of lead-free solders bearing micro and nano particles, vol. 82, no. 1, pp. 1-32, 2014.

[6] IPC, "Round Robin Testing and Analysis of Lead Free Solder Pastes with Alloys of Tin, Silver, Copper" – Final Report," IPC Solder Products Value Council, Chicago, IL, 2016.

[7] W. J. Plumbridge, Second Generation Lead-free Solder Alloys – A Challenge to Thermodynamics, vol. 136, no. 11, pp. 1811-1821, 2005.

[8] R. Schueller, N. Blattau, J. Arnold and P. Craig Hillman, "Second Generation Pb-free alloys," in SMTA Journal, College Park, MD, USA, 2010.

[9] F. Ji, L. Z. X S B, L. Gao, Z. Sheng and W. Dai, "Reliability Evaluation of QFN Devices Soldered Joints with Creep Model," Chinese Journal of Mechanical Engineering (CJME), vol. 24, no. 03, p. 428, 2011.

[10] L. Sun, L. Zhang, S. J. Zhong, J. Ma and L. Bao, "Reliability study of industry Sn3.0Ag0.5Cu/Cu lead-free soldered joints in electronic packaging," Journal of Materials Science: Materials in Electronics, vol. 26, no. 11, pp. 9164-9170, 2015.

[11] P. Choudhury, M. Ribas, R. Pandher, A. Kumar, S. Mukherjee, S. Sarkar and B. Singh, "Development of Lead-Free Alloys with Ultra-High Thermo- Mechanical Reliability," SMTA International, pp. 128-133, 1 10 2015.

[12] R. S. Pandher, B. G. Lewis, R. Vangaveti and B. Singh, "Drop Shock Reliability of Lead-Free Alloys - Effect of Micro-Additives," 2007 Proceedings 57th Electronic Components and Technology Conference, pp. 669-676, 2007.

[13] L. Yang, J. Ge, H. Liu, L. Xu and A. Bo, "Effect of Cooling Rate on the Microstructure and Mechanical Properties of Sn-1.0Ag-0.5Cu–0.2BaTiO3 Composite Solder," Journal of Electronic Materials, vol. 44, no. 11, pp. 4595-4603, 2015.

[14] Z. Liang, G. Yonghuan, S. Lei and H. Chengwena, "Reliability of SnAgCuFe Solder Joints in WLCSP30 Device," Rare Metal Materials and Engineering, vol. 45, no. 11, pp. 2823-2826, 2016.

[15] D. Frear, L. N. Ramanathan, J. W. Jang and N. L. Owen, "Emerging reliability challenges in electronic packaging," in IEEE International Reliability Physics Symposium Proceedings, Phoenix, AZ, USA, 2008.

[16] H. Li, T. An, X. Bie, G. Shi and F. Qin, "Thermal fatigue reliability analysis of PBGA with Sn63Pb37 solder joints," in 2016 17th International Conference on Electronic Packaging Technology (ICEPT) Cite this publication, Wuhan, China, 2016.

[17] E. Lechovič, E. Hodúlová, B. Szewczyková, I. KovaříKová and K. Ulrich, "Solder Joint Reliability," in Institute of Production Technologies, Faculty of Materials Science and Technology, Slovak University of Technology, Trnava, Slovak Republic, 2009.

[18] C. Shen, Z. Hai, C. Zhao, J. Zhang, J. L. Evans, M. J. Bozack and J. C. Suhling, "Packaging Reliability Effect of ENIG and ENEPIG Surface Finishes in Board Level Thermal Test under Long-Term Aging and Cycling," NCBI, vol. 10, no. 5, p. 451, May 2017.

[19] D. A. Shnawah, M. F. Mohd and S. A. Badruddin, "A review on thermal cycling and drop impact reliability of SAC solder joint in portable electronic products," Microelectronics Reliability, vol. 52, no. 1, pp. 90-99, January 2012.

[20] M. Alam, Y. Chana and K. Tu, "Elimination of Au-embrittlement in solder joints on Au/Ni metallization," Materials Research Society, vol. 19, no. 5, pp. 1303-1306, May 2004.

[21] D. Shangguan, "Lead-Free Solder Interconnect Reliability," ASM International, pp. 1-21, 2005.

[22] C. Chen, F. Hou, F. Liu, Q. She, L. Cao and L. Wan, "Thermo-mechanical reliability analysis of a RF SiP module based on LTCC substrate," Microelectronics Reliability, vol. 79, pp. 38-47, December 2017.

[23] M. Forde, K. Manning and S. Kudtarkar, "Solder Joint Reliability: An Integrated Study of Electromigration, Thermal Migration and Thermo- Mechanical Effects," in Integrated Reliability Workshop Final Report (IRW), 2012 IEEE International, South Lake Tahoe, CA, USA, 2012.

[24] J. Xian, G. Zenga, S. Belyakov, Q. Gu, K. Nogita and C. Gourlay, "Anisotropic thermal expansion of Ni3Sn4, Ag3Sn, Cu3Sn, Cu6Sn5 and βSn," Elsevier, vol. 91, pp. 50-64, 17 August 2017.

[25] O. Ogbomo, E. H. Amalu, N. Ekere and P. Olagbegi, "Effect of Coefficient of Thermal Expansion (CTE) Mismatch of Solder Joint Materials in Photovoltaic (PV) Modules Operating in Elevated Temperature Climate on the Joint's Damage," in 27th International Conference on Flexible Automation and Intelligent Manufacturing, FAIM2017, Modena, Italy, 2017.

[26] A. Kanjilal and P. Kumar, "Growth of Interfacial Intermetallic Compound Layer in Diffusion-Bonded SAC–Cu Solder Joints During Different Types of Thermomechanical Excursion," in Journal of Electronic Materials, Bangalore, 2017.

[27] E. Liu, T. Zahner, S. Besold and G. Elger, "Location resolved transient thermal analysis to investigate crack growth in solder joints," in 016 22nd International Workshop on Thermal Investigations of ICs and Systems (THERMINIC), Budapest, 2016.

[28] X. Li, R. Sun and Y. Wang, "A review of typical thermal fatigue failure models for solder joints of electronic components," Materials Science and Engineering, vol. 242, pp. 1-5, September 2017.

[29] M. Shirator, Q. Yu and D.-S. Kim, "The Effect of Inter-metallic Compound on Thermal Fatigue Reliability of Lead-Free Solder Joints(Electronic Devices)," in Proceedings of the Asian Pacific Conference on Fracture and Strength and International Conference on Advanced Technology in Experimental Mechanics, Yokohama, 2017.

[30] R. Tilgner, "Physics of failure for interconnect structures: an essay," Microsystem Technologies, vol. 15, no. 1, pp. 129-138, January 2009.

[31] C. Basaran and R. Chandaroy, "Using Finite element analysis for simulation of reliability tests on solder joints in microelectronic packaging," Computers & Structures, vol. 74, no. 2, pp. 215-231, January 2000.

[32] S. Mallik and F. Kaiser, "Reliability Study of Subsea Electronic Systems Subjected to Accelerated Thermal Cycle Ageing," International Association of Engineers, pp. 1-4, 2-4 July 2014.

[33] S. Y. Yang, I. Kim and S.-B. Lee, "A Study on the Thermal Fatigue Behavior of Solder Joints Under Power Cycling Conditions," IEEE Transactions on Components and Packaging Technologies, vol. 31, no. 1, pp. 3-12, 2008.

[34] Choi, C. & Dasgupta, A., “Fatigue of Solder Interconnects in Microelectronic Assemblies under Random Vibration”. Maryland, Elsevier, pp. 165-16, 2014.

[35] Y. Shen, "Thermo-mechanical Stresses in Copper Interconnects -A Modelling Analysis," Microelectronic Engineering, vol. 83, pp. 446-459, 2006.

[36] J. Lau, Thermal Stress and Strain in Microelectronics Packaging, vol. 13, V. N. Reinhold, Ed., New York, USA: Springer, 1993, p. 114.

[37] N. Noda, R. B. Hetnarski and Y. Tanigawa, Thermal Stresses, New York: Taylor & Francis, 2003.

[38] R. J. Coyle, K. Sweatman and B. Arfaei, "Thermal Fatigue Evaluation of Pb-Free Solder Joints: Results, Lessons Learned, and Future Trends," The Journal of The Minerals, Metals & Materials Society (TMS), vol. 67, no. 10, pp. 2394-2415, October 2015.

[39] C. Huang, D. Yang, B. Wu, L. Liang and Y. Yang, "Failure mode of SAC305 lead-free solder joint under thermal stress," in 2012 International Conference on Electronic Packaging Technology & High Density Packaging, China, 2012.

[40] M. J. Magnien, "Investigation of Mechanical Behavior and Failure Mechanisms in Miniaturized Solder Interconnects“," University of Vienna, Vienna, 2015.

[41] G. Petrone, C. Barbagallo and M. Scionti, "Thermo-Mechanical Analysis and Fatigue Life Prediction for an Electronic Surface-Mount Device (SMD)," in Proceedings of the 2015 COMSOL Conference in Grenoble, Catania, Italy, 2015.

[42] V. Gektin, A. Bar-Cohen and J. Ames, "Coffin-Manson fatigue model of underfilled flip-chips," IEEE Transactions on Components, Packaging, and Manufacturing Technology: Part A, vol. 20, no. 3, pp. 317-326, September 1997.

[43] M. Pecht and A. Dasgupta, "Physics-of-failure: an approach to reliable product development," IEEE 1995 International Integrated Reliability Workshop. Final Report, pp. 1-4, 22-25 October 1995.

[44] P. Chauhan, M. Osterman, S. W. R. Lee and M. Pecht, "Critical Review of the Engelmaier Model for Solder Joint Creep Fatigue Reliability," IEEE Transactions on Components and Packaging Technologies, vol. 32, no. 3, pp. 693-700, September 2009.

[45] S.-P. Zhu, P. Yue, Z.-Y. Yu and Q. Wang, "A Combined High and Low Cycle Fatigue Model for Life Prediction of Turbine Blades," Materials (Basel), vol. 10, no. 7, pp. 698-704, 2017.

[46] S. Knecht and L. Fox, "Integrated matrix creep: application to accelerated testing and lifetime prediction," in Solder joint reliability theory and applications, vol. Chapter 16, New York, Van Nostrand Reinhold, 1991, p. Chapter 6.

[47] T. Pan, "Critical accumulated strain energy (case) failure criterion for thermal cycling fatigue of solder joints," Journal of Electronic Packaging, Transactions of the ASME, vol. 116, no. 8, pp. 163-170, 1994.

[48] V. Stolkarts, B. Moran and L. Keer, "Constitutive and damage model for solders," in Electronic Components and Technology Conference, 1998.

[49] F. Q. Sun, J. C. Liu, Z. Q. Cao, X. Y. Li and T. M. Jiang, "Modified Norris–Landzberg Model and Optimum Design of Temperature Cycling Alt," Strength of Materials, vol. 48, no. 1, pp. 135-145, January 2016.

[50] H. Fei, K. Yazzie, N. Chawla and H. Jiangi, "Modeling Fracture of Sn-Rich (Pb-Free) Solder Joints Under Mechanical Shock Conditions," Journal of Electroniv Materials, pp. 1-11, 2012.

[51] V. Tvergaard, "Influence of voids on shear band instabilities under plane strain conditions," International Journal of Fracture, vol. 17, no. 4, pp. 389-407, 1981.

[52] H. Fel, K. Yazzie, N. Chawla and H. Jiang, "The Effect of Random Voids in the Modified Gurson Model," Journal of Electronic Materials, vol. 41, no. 2, pp. 177-183, 2011.

[53] A. Gurson, "Continuum Theory of Ductile Rupture by Void Nucleation and Growth: Part I—Yield Criteria and Flow Rules for Porous Ductile Media," Journal of Engineering Materials and Technology, vol. 99, no. 1, pp. 2-15, 1977.

[54] G. Tang, B. An, Y. Wu and F. Wu, "Finite Element Analysis of Sn-Ag-Cu Solder Joint Failure under Impact Test," 2009 International Conference on Electronic Packaging Technology & High Density Packaging, no. 67, pp. 1220-1224, 13 August 2009.

[55] L. Xi and Z. Songlin, "Changes in mechanical properties of vehicle components after strengthening under low-amplitude loads below the fatigue limit," Fatigue and Fracture of Engineering Materials and Structures, vol. 31, no. 10, pp. 847-855, 9 September 2009.

[56] N. E. Dowling, Mechanical Behavior of Materials, 4th ed., K. S. Prasad and R. Narayanasamy, Eds., Essex, England: Pearson Education Limited, 2013, pp. 40-802.

[57] E. Santecchia, A. M. S. Hamouda, F. Musharavati, E. Zalnezhad, M. Cabibbo, M. E. Mehtedi and S. Spigarelli3, "A Review on Fatigue Life Prediction Methods for Metals," Advances in Materials Science and Engineering, pp. 1-26, 2016.

[58] M. A. Miner, "Cumulative damage in fatigue," Journal of Applied Mechanics, vol. 12, pp. A159-A164, 1945.

[59] G. Ayoub, M. Naït-abdelaziz, F.Zaïri and J. Gloaguenac, "Multiaxial fatigue life prediction of rubber-like materials using the continuum damage mechanics approach," Procedia Engineering, vol. 2, no. 1, pp. 985-993, April 2010.

[60] S. Suresh, Fatigue of Materials, Cambridge, UK: Cambridge University Press, 1991.

[61] A. Palmgren, "Die lebensdauer von kugellagern," Zeitschrift des Vereins Deutscher Ingenieure,, vol. 68, pp. 339-341, 1924.

[62] R. P. Skelton, T. Vilhelmsen and G. A. Webster, "Energy criteria and cumulative damage during fatigue crack growth," International Journal of Fatigue, vol. 20, no. 9, pp. 641-649, 1998.

[63] M. Newby, "Estimation of Paris-Erdogan law parameters and the influence of environmental factors on crack growth," International Journal of Fatigue, vol. 13, no. 4, pp. 291-301, 1991.

[64] G. S. Wang, "An EPFM analysis of crack initiation, stable growth and instability," Engineering Fracture Mechanics, vol. 50, no. 2, pp. 261-282, 1995.

[65] J. R. Rice, "A path independent integral and the approximate analysis of strain concentration by notches and cracks," Journal of Applied Mechanics, vol. 35, no. 2, pp. 379-386, 1968.

[66] S. Wiese, S. Jakschik, F. Feustel and E. Meusel, "Fracture behaviour of flip chip solder joints," 2001 Proceedings. 51st Electronic Components and Technology Conference (Cat. No.01CH37220), pp. 1299-1306, 01 June 2001.

[67] Z. Guo and H. Conrad, "Fatigue Crack Growth Rate in 63Sn37Pb Solder Joints," Journal of Electronic Packaging, vol. 115, no. 2, pp. 1-6, 01 June 1993.

[68] Q. Zhang, A. Dasgupta and P. Haswell, "Isothermal Mechanical Durability of Three Selected PB-Free Solders: Sn3.9Ag0.6Cu, Sn3.5Ag, and Sn0.7Cu," Journal of Electronic Packaging, vol. 127, no. 4, pp. 512-522, 03 May 2005.

[69] C. DeMilo, C. Bergad, R. Forni and T. Brukilacchio, "Thermally Induced Stresses Resulting from Coefficient of Thermal Expansion Differentials Between an LED Sub-Mount Material and Various Mounting Substrates. Integrated Optoelectronic Devices," International Society for Optics and Photonics, no. doi: 10.1117/12.697489, 2007.

[70] Y. Zhang, Z. Cai, J. C. Suhling, P. Lall and M. J. Bozack, "The effects of aging temperature on SAC solder joint material behavior and reliability," 58th IEEE Electronic Components and Technology Conference (2008), pp. 99-112, 27-30 May 2008.

[71] IDC Technologies, www.idc-online.com, 2018.[Online]. Available:http://www.idc online.com/technical_references/pdfs/mechanical_engineering/Failure_in_Solder_Joints.pdf.

[72] J. Hwang and R. Vargas, "Solder Joint Reliability—Can Solder Creep?," Soldering & Surface Mount Technology, vol. 2, no. 2, pp. 38-45, 1990.

[73] Y. Lee and C. Basaran, "A Creep Model for Solder Alloys," Journal of Electronic Packaging, vol. 133, no. 4, pp. 1-18, December 2011.

[74] C.-C. Lee, K.-S. Ka, R.-S. Cheng, C.-J. Zhan and T.-C. Chang, "Reliability enhancements of chip-on-chip package with layout designs of microbumps," Elsevier, vol. 120, pp. 138-145, 25 May 2014.

[75] J. Weertman, "Steady - State Creep through Dislocation Climb," Journal of Applied Physics, vol. 28, no. 3, 1957.

[76] C. Herring, "Diffusional viscosity of a polycrystalline solid," Journal of Applied Physics, vol. 21, no. 5, pp. 437-445, 1950.

[77] E. H. Wong, Y.-W. Mai, R. Rajoo, K. T. Tsai, F. Liu, S. K. W. Seah and C.-L. Yeh, "Micro Impact Characterization of Solder Joint for Drop Impact Application," in IEEE, San Diego, CA, USA, 2006.

[78] C.-C. Lee, K.-C. Chang and Y.-W. Yang, "Lead-free solder joint reliability estimation of flip chip package using FEM-based sensitivity analysis," Soldering & Surface Mount Technology, vol. 21, no. 1, pp. 31-41, 2009.

[79] S. F. Choudhury, "Intermetallic Compounds and Their Effects on the Mechanical Performance of Micro Scale Solder Bonds," Soud F. Choudhury, Connecticut, 2016.

[80] J. Gomez and C. Basaran, "Damage Mechanics Constitutive Model for Pb/Sn Solder Joints Incorporating Nonlinear Kinematic Hardening and Rate Dependent Effects Using a Return Mapping Integration Algorithm," Mechanics of Materials, vol. 38, pp. 585-598, July 2006.

[81] C. Basaran, H. Ye, D. C. Hopkins, D. Frear and J. K. Lin, "Failure Modes of Flip Chip Solder Joints Under High Electric Current Density," Journal of Electronic Packaging, vol. 127, no. 2, pp. 157-163, 15 September 2004.

[82] Y. Zhu, X. Li, C. Wang and R. Gao, "A new creep–fatigue life model of lead-free solder joint," Microelectronics Reliability, vol. 55, no. 7, pp. 1097-1100, June 2015.

[83] V. Ramachandran and K.-N. Chiang, "Feasibility Evaluation of Creep Model for Failure Assessment of Solder Joint Reliability of Wafer-Level Packaging," IEEE Transactions on Device and Materials Reliability, vol. 17, no. 4, pp. 672-677, December 2017.

[84] B. Kashyap and G. Murty, “Experimental constitutive relations for the high temperature deformation of a Pb□Sn eutectic alloy,” Materials Science and Engineering, vol. 50, no. 2, pp. 205-213, 1981.

[85] P. L. Hacke, A. F. Sprecher and H. Conrad, “Modeling of the Thermomechanical Fatigue of 63Sn-37Pb Alloy,” Thermo-mechanical Fatigue Behavior of Materials,” ASTM STP 1186, pp. 91-105, 1993.

[86] L. Anand, "Constitutive Equations for Hot Working of Metals," International Journal of Plasticity, vol. 1, no. 3, pp. 213-231, 1985.

[87] S. B. Brown, K. H. Kim and L. Anand, “An internal variable constitutive model for hot working of metals,” International Journal of Plasticity, vol. 5, no. 2, pp. 95-130, 1989.

[88] T. Pan, “Thermal Cycling Induced Plastic Deformation in Solder Joints-Part 11: Accumulated Deformation in Through Hole Joint,” IEEE Transactions on Components, Hybrids, and Manufacturing Technology, vol. 14, no. 4, pp. 824-832, December 1991.

[89] Y. Lee and C. Basaran, “A Creep Model for Solder Alloys,” Journal of Electronic Packaging, vol. 133, no. 4, pp. 1-18, December 2011.

[90] X. Q. Shi, Z. P. Wang, Q. J. Yang and H. L. J. Pang, “Creep Behavior and Deformation Mechanism Map of Sn-Pb Eutectic Solder Alloy,” Journal of Engineering Materials and Technology, vol. 125, no. 1, pp. 81-88, 31 December 2002.

[91] M. Motalab, Z. Cai, J. C. Suhling and P. Lall, “Determination of Anand constants for SAC solders using stress-strain or creep data,” in 13th IEEE Intersociety Conference on Thermal and Thermomechanical Phenomena in Electronic Systems (ITherm), Auburn, 2012.

[92] C. Huang, D. Yang, B. Wu, L. Liang and Y. Yang, "Failure mode of SAC305 lead-free solder joint under thermal stress," in 2012 International Conference on Electronic Packaging Technology & High Density Packaging, China, 2012.

[93] S. Tay, A. Haseeb, M. R. Johan, P. Munroe and M. Quadir, "Influence of Ni nanoparticle on the morphology and growth of interfacial intermetallic compounds between Sne3.8Age0.7Cu lead-free solder and copper substrate," Intermetallics, pp. 8-15, 2013.

[94] A. Zbrzezny, A. Snugovsky and D. Perovic, "Impact of board and component metallizations on microstructure and reliability of lead-free solder joints," Microelectronics Reliability, vol. 12, pp. 2205-2214, 2007.

[95] Y. Xing, J. Woods and E. Cotts, "Understanding lead free solder damage : time dependence of SnAgCu microstructure and thermomechanical response," UIC Consortium Presentation, vol. 10, pp. 693-700, 2005.

[96] D. A. Şerban, E. Linul, C. S. Nes and L. Marsavina, "Numerical Modelling of Damage and Failure of Ductile Materials in Finite Element Analysis," Universităţii Petrol – Gaze din Ploieşti, pp. 11-20, 2015.

[97] A. I. Karayan, D. Ferdian, S. Harjanto, D. M. Nurjaya, A. Ashari and H. Castaneda, "Finite Element Analysis Applications," in Finite Element Analysis - Applications in Mechanical Engineering, InTechOpen, 2012, pp. 217-234.

[98] R. D. Borst and L. M. H.-B. P. J. Sluys, "Fundamental Issues In Finite Element Analyses Of Localization Of Deformation Engineering Computations," Int J for Computer-Aided Engineering, vol. 10, no. 2, pp. 99-121(23), 1993.

[99] M. Ortiz, Y. Leroy and A. Needleman, "A finite element method for localized failure analysis,Computer Methods in Applied Mechanics and Engineering," Journal of Computer Methods in Applied Mechanics and Engineering, vol. 61, no. 2, pp. 189-214, March 1987.

[100] F. X. Che and J. H. L. Pang, "Study on Board-Level Drop Impact Reliability of Sn–Ag–Cu Solder Joint by Considering Strain Rate Dependent Properties of Solder," IEEE Transactions on Device and Materials Reliability, vol. 15, no. 2, pp. 181-190, 2015.

[101] G. Petrone et al., Modelling and Simulation, 391-417, I-Tech Education and Publishing, Croatia (2008).